

Drag Coefficient of a Rigid Spherical Particle in a Near-Critical Binary Fluid Mixture beyond the Regime of the Gaussian Model

Shunsuke Yabunaka^{1†}, and Youhei Fujitani^{2‡}

¹Department of Physics, Kyushu University, Fukuoka 819-0395, Japan

²School of Fundamental Science and Technology, Keio University, Yokohama 223-8522, Japan

(Received xx; revised xx; accepted xx)

The drag coefficient of a rigid spherical particle deviates from the Stokes law when it is put into a near-critical fluid mixture in the homogeneous phase with the critical composition. The deviation ($\Delta\gamma_d$) is experimentally shown to depend approximately linearly on the correlation length of the composition fluctuation far from the particle (ξ_∞), and is suggested to be caused by the preferential adsorption between one component and the particle surface. In contrast, the dependence was shown to be much steeper in the previous theoretical studies based on the Gaussian free-energy density. In the vicinity of the particle, especially when the adsorption of the preferred component makes the composition strongly off-critical, the correlation length becomes very small as compared with ξ_∞ . This spacial inhomogeneity, not considered in the previous theoretical studies, can influence the dependence of $\Delta\gamma_d$ on ξ_∞ . To examine this possibility, we here apply the renormalized local functional theory, describing the preferential adsorption in terms of the surface field. This theory was previously proposed to explain the interaction of walls immersed in a (near-)critical binary fluid mixture. The free-energy density in this theory, coarse-grained up to the local correlation length, has much complicated dependence on the order parameter, as compared with the Gaussian free-energy density. Still, a concise expression of the drag coefficient, which was derived in one of the previous theoretical studies, turns out to be available in the present formulation. We show that, as ξ_∞ becomes larger, the dependence of $\Delta\gamma_d$ on ξ_∞ becomes distinctly gradual and close to the linear dependence.

1. Introduction

Brownian motion has been one of the main topics in the physics for a long time (Bian *et al.* 2016). When a rigid spherical particle moves translationally at a sufficiently low constant speed in a quiescent one-component fluid, the fluid exerts a drag force, whose magnitude is proportional to the particle speed. The constant of proportionality, called the drag coefficient, is given by $6\pi\eta_0 a$, where η_0 is the fluid viscosity and a is the particle radius, according to the Stokes law (Stokes 1851). The self-diffusion coefficient of a colloidal particle is usually equal to $k_B T$ divided by the drag coefficient (Sutherland 1905; Einstein 1905), where k_B is the Boltzmann constant and T is the temperature of the fluid. This relation (Einstein's relation) can be derived from a linear Langevin equation for the particle velocity even if it is generalized to have the memory kernel representing the back-flow effect (Zwanzig & Bixon 1970; Zwanzig & Bixon 1975; Widom 1971; Case 1971;

† Email address for correspondence: yabunaka123@gmail.com

‡ Email address for correspondence: youhei@appi.keio.ac.jp

Kubo *et al.* 1991). A Brownian particle has been used experimentally as a probe for local environments in the field of microrheology (Brau *et al.* 2007; Pesce *et al.* 2009; Kimura 2009; Bertseva *et al.* 2012; Grebenkov *et al.* 2013; Domínguez-García *et al.* 2014). The trajectory of an optically trapped Brownian particle can be measured with resolutions of nanometers and microseconds (Lukić *et al.* 2005; Franosch *et al.* 2011; Huang *et al.* 2011; Grimm *et al.* 2012).

Some properties of a binary fluid mixture in the homogeneous phase near the demixing critical point can be also probed by a Brownian particle in the mixture (Bonn *et al.* 2009; Mazur & van der Zwan 1978; van der Zwan & Mazur 1979; Furukawa *et al.* 2013; Barbot & Araki 2017; Camley & Brown 2014; Tani & Fujitani 2018). Although it is not always the case (Beysens 2019), the particle surface usually attracts one of the two components more; this preferential adsorption can be described using a surface field in a coarse-grained picture. As a result, the preferred component is absorbed near the particle surface; the composition deviation from the composition in the bulk decays very slowly in the adsorption layer, which extends from the surface by the thickness comparable with the correlation length of the composition fluctuation in the bulk (Cahn 1977; Binder 1983; Beysens & Leibler 1982; Beysens & Estève 1985; Holyst & Poniewierski 1987). It has been observed that the self-diffusion coefficient of a particle, put in a mixture with the critical composition, becomes smaller as the critical temperature is approached on the side of the homogeneous phase (Bal'tsevich *et al.* 1967; Martynets & Matizen 1970; Lyons *et al.* 1973, 1974; Lee 1976; Omari *et al.* 2009). Let us write γ_d , $\Delta\gamma_d \equiv \gamma_d - 6\pi\eta_0 a$, and ξ_∞ for the drag coefficient, the deviation of γ_d from the Stokes law, and the correlation length far from the particle, respectively. Some researchers (Lee 1976; Omari *et al.* 2009) interpret their data suggesting the linear dependence of $\Delta\gamma_d$ on ξ_∞ by assuming the particle radius to be effectively enlarged by the thickness of the adsorption layer, which is on the order of ξ_∞ . Clearly, however, the adsorption layer is not a part of a rigid particle; it can be deformed and is open to fluid flows. It is thus necessary to explain the deviation in terms of the hydrodynamics which can describe the flow in the adsorption layer. In this line of study, Okamoto *et al.* (Okamoto *et al.* 2013) employed the hydrodynamics based on the Gaussian free-energy density with the surface field being considered, and revealed that the osmotic pressure due to the composition gradient around the particle can cause the deviation. However, their result of $\Delta\gamma_d$ is proportional to ξ_∞^6 , which is much steeper than the observed dependence. Their calculation, supposing sufficiently weak adsorption, was extended to treat strong adsorption in the framework based on the Gaussian free-energy density in (Fujitani 2018), where the dependence of $\Delta\gamma_d$ on ξ_∞ is still shown to be steeper than linear. The Gaussian model used in these previous studies supposes a small and homogeneous correlation length. However, as the adsorption is stronger, the correlation length of the fluctuation near the particle becomes smaller than ξ_∞ because the average composition there becomes farther from the critical composition, which is realized far from the particle (Okamoto & Onuki 2012). This inhomogeneity can reduce the dependence of $\Delta\gamma_d$ on ξ_∞ from the one in the Gaussian model.

After giving a brief review on the conventional Stokes law in Sect. 2, we apply the renormalized local functional theory to consider the inhomogeneity in a near-critical binary fluid mixture, instead of the Gaussian model used previously. This theory was originally proposed by Fisher and Au-Yang (Fisher & Au-Yang 1980) for static properties of binary fluid mixtures at the critical point and extended by Okamoto and Onuki (Okamoto & Onuki 2012) to describe those near the critical point. In this theory, the free-energy density of the Ginzburg-Landau-Wilson type is coarse-grained up to the local fluctuation correlation length, as mentioned in Sect. 3.1. From this density, the

hydrodynamics for the length scales larger than the local correlation length can be formulated (Yabunaka *et al.* 2015), which is mentioned in Sect. 3.2. The procedure of formulating the hydrodynamics is the same as in the model H (a standard model for the critical dynamics)(Hohenberg & Halperin 1977; Onuki 2002); the thermal noise need not be considered here for the dynamics at the large length scales (Okamoto *et al.* 2013; Furukawa *et al.* 2013). In fact, considering the thermal noise in a near-critical mixture does not change the Stokes law in the absence of the preferential adsorption, according to (Mazur & van der Zwan 1978). The Gaussian free-energy density is composed of a quadratic function with respect to the order parameter and the square gradient term, while the density is much more complicated in the renormalized local functional theory. Still, a concise expression of the drag coefficient, which was previously derived in the Gaussian model (Fujitani 2018), is shown in Sect. 3.3 to remain available in the present study. The perturbation with respect to a dimensionless surface field, employed in (Fujitani 2018), is not available here. We instead devise an alternative procedure in Sect. 4.1. Two points peculiar to our calculation are stated in the rest of Sect. 4. Our results are shown in Sect. 5, and are discussed in Sect. 6.

2. Preliminaries

In this section, we assume that a rigid spherical particle undergoes translational motion with a constant velocity in a quiescent incompressible fluid which can be regarded as a one-component fluid, to review a hydrodynamic derivation of the conventional Stokes law. The derivation below can be extended straightforwardly for our problem discussed in the subsequent sections. See (Bedeaux & Mazur 1974) for the derivation from the linearized equations in the fluctuating hydrodynamics, and (Itami & Sasa 2015) for the one from the Hamilton dynamics of many particle systems within the linear response regime.

The space and time variables are denoted by (\mathbf{x}, t) ; ρ_o and η_o respectively denote the mass density and the viscosity of the ambient fluid. Its velocity and pressure fields, \mathbf{v} and p , satisfy the incompressibility condition and the Navier-Stokes equation, *i.e.*,

$$0 = \nabla \cdot \mathbf{v} \quad \text{and} \quad \rho_o \frac{D\mathbf{v}}{Dt} = -\nabla p + \eta_o \Delta \mathbf{v}, \quad (2.1)$$

where $D/(Dt)$ implies the Lagrangian time-derivative. The no-slip boundary condition is imposed at the particle surface.

We write a and $U_o \mathbf{e}_z$ for the particle radius and the particle velocity, respectively, where \mathbf{e}_z denotes a unit vector. The fields are stationary if viewed on the frame co-moving with the particle, where the space and time variables are denoted by (\mathbf{x}', t') . Because of $\mathbf{x}' = \mathbf{x} - U_o t \mathbf{e}_z$ and $t' = t$, the second entry of (2.1) becomes

$$\rho \mathbf{v}' \cdot \nabla' \mathbf{v}' = -\nabla' p' + \eta_o \Delta' \mathbf{v}', \quad (2.2)$$

where $\mathbf{v}' = \mathbf{v} - U_o \mathbf{e}_z$ and $p' = p$ are the fields on the co-moving frame, and ∇' and Δ' are the differential operators with respect to \mathbf{x}' . We can non-dimensionalize the fields by using ρ_o , a and U_o to have the Reynolds number. Assuming the low Reynolds number (Chester *et al.* 1976; Hutter & Wang 2016), we neglect the left-hand side of (2.2), and thus that of the second entry of (2.1). The resultant equation is the Stokes equation on the original frame. Linearizing the governing equations in this way, we obtain \mathbf{v} and p up to the linear order of the particle velocity to calculate the drag coefficient.

The linearization above is also attainable without explicit non-dimensionalization if we use εU instead of U_o , where U is a nonzero constant with the dimension of speed and ε is

a dimensionless parameter. What to do for the linearization with respect to the particle speed is to expand \mathbf{v} and p with respect to ε and perform calculations only up to the order of ε . Although ε is known to represent the Reynolds number in this example, we need not specify this physical meaning for calculating the drag coefficient, which is the ratio of the magnitude of the drag force to the particle speed in the limit of $\varepsilon \rightarrow 0$. We define $\mathbf{v}^{(1)}$ and $p^{(1)}$ so that

$$\mathbf{v} = \varepsilon \mathbf{v}^{(1)} \quad \text{and} \quad p = p^{(0)} + \varepsilon p^{(1)} \quad (2.3)$$

hold up to the order of ε , where the static pressure $p^{(0)}$ is a constant. Using the co-moving frame transiently, as in the preceding paragraph, we have the incompressibility condition and Stokes equation for $\mathbf{v}^{(1)}$ and $p^{(1)}$. The solution in (Lamb 1932) is available as it is in calculating the drag coefficient, but we here show an alternative way to prepare for the calculations in the subsequent sections.

We set the spherical polar coordinate system (r, θ, ϕ) so that the polar axis (z -axis) is along \mathbf{e}_z , and consider the instance that the particle center passes the origin. Because of the symmetry of the particle motion, we use a spherical harmonics $Y_{10}(\theta) = \sqrt{3/(4\pi)} \cos \theta$ to express the angular dependence of $p^{(1)}$ as

$$p^{(1)}(\mathbf{x}) = p_{10}(r) Y_{10}(\theta) , \quad (2.4)$$

whereby p_{10} is defined. Using the vector spherical harmonics for that of $\mathbf{v}^{(1)}$ (Fujitani 2007), we define R_{10} and T_{10} so that

$$v_r^{(1)}(\mathbf{x}) = R_{10}(r) Y_{10}(\theta) , \quad v_\theta^{(1)}(\mathbf{x}) = \frac{T_{10}(r)}{\sqrt{2}} \partial_\theta Y_{10}(\theta) , \quad \text{and} \quad v_\phi^{(1)}(\mathbf{x}) = 0 \quad (2.5)$$

hold, where ∂_θ denotes $\partial/(\partial\theta)$ and the time variable is dropped because only the particular time is considered. Noting that the incompressibility condition gives

$$T_{10} = \frac{1}{r\sqrt{2}} \partial_r r^2 R_{10} , \quad (2.6)$$

we eliminate p_{10} from the r and θ -components of the Stokes equation to have

$$(\rho \partial_\rho + 1)(\rho \partial_\rho - 2)(\rho \partial_\rho + 3)(\rho \partial_\rho) \mathcal{R}(\rho) = 0 , \quad (2.7)$$

where we use a dimensionless radial distance $\rho = r/a$ and dimensionless function,

$$\mathcal{R}(\rho) = \frac{R_{10}(r)}{U} \sqrt{\frac{3}{4\pi}} . \quad (2.8)$$

The boundary conditions are

$$\mathbf{v} = \varepsilon U \mathbf{e}_z \text{ at } r = a \quad \text{and} \quad \mathbf{v} \rightarrow 0 \text{ as } r \rightarrow \infty . \quad (2.9)$$

The former represents the no-slip boundary condition at the surface, which gives $R_{10} = T_{10}/\sqrt{2} = \sqrt{4\pi/3} U$ at $r = a$. Thus, we use (2.6) to obtain

$$\mathcal{R} = 1 \text{ and } \partial_\rho \mathcal{R} = 0 \text{ at } \rho = 1 \quad \text{and} \quad \mathcal{R} \rightarrow 0 \text{ as } \rho \rightarrow \infty . \quad (2.10)$$

Noting that the four operators inside the respective pairs of parentheses in (2.7) are commutable, we find that \mathcal{R} is given by a linear combination of ρ^{-1} and ρ^{-3} . The respective coefficients are found to be $3/2$ and $-1/2$ with the aid of the surface boundary conditions in (2.10). We thus have $\mathcal{R}(\rho) = 1 + \alpha_0(\rho)$, where α_0 is defined as

$$\alpha_0(\rho) = \frac{3}{2\rho} - \frac{1}{2\rho^3} - 1 \quad (2.11)$$

for later convenience.

We write \mathbf{E} for the rate-of-strain tensor; $E_{xz} = (\partial_x v_z + \partial_z v_x)/2$, for example. The drag force is along \mathbf{e}_z ; its z component is given by the surface integral of

$$\mathbf{e}_z \cdot (-p\mathbf{1} + 2\eta_0\mathbf{E}) \cdot \mathbf{e}_r \quad (2.12)$$

over the particle surface. Here, $\mathbf{1}$ denotes the isotropic tensor and \mathbf{e}_r is the unit vector in the radial direction. Through the θ -component of the Stokes equation at the order of ε , p_{10} is linked with \mathcal{R} with the aid of (2.5) and (2.6). We thus find the z -component of the drag force at the order of ε to be given by

$$-\frac{4\pi}{3}\eta_0 a \varepsilon U \left(\frac{1}{2}\partial_\rho^3 + 2\partial_\rho^2 - 2\partial_\rho \right) \mathcal{R} \quad (2.13)$$

evaluated at $\rho = 1$ (Fujitani 2007; Okamoto *et al.* 2013). The term $-2\partial_\rho\mathcal{R}$ vanishes because of (2.10). Substituting $\mathcal{R}(\rho) = 1 + \alpha_0(\rho)$ into the above and dividing the result by εU give the Stokes law.

To consider how the Stokes law is modified by the preferential adsorption in the near criticality, we should add a term, representing the force caused by the composition gradient, to the Stokes equation. As shown in Sect. 3.2, this force can be calculated from the free-energy density for the mixture, which is given by the integrand of the first integral of (3.1) in the next section.

3. Formulation for a near-critical binary fluid mixture

Suppose a near-critical binary fluid mixture with the critical composition in the homogeneous phase; T is assumed to be homogeneous and close to the critical temperature T_c . The reduced temperature is defined as $\tau \equiv |T - T_c|/T_c > 0$. The composition is here represented by the difference between the mass densities of the two components, which is denoted by φ . We define ψ as $\varphi - \varphi_c$, where φ_c represents the critical composition. In the mixture bulk at the equilibrium, the order parameter ψ fluctuates around zero significantly on length scales smaller than the correlation length, and the thermal average of φ equals φ_c . On larger length scales, we can neglect the fluctuation about the coarse-grained equilibrium profile of the order parameter, which can deviate from zero near a wall or a surface in contact with the mixture because of the preferential adsorption. We assume the binary fluid mixture to be incompressible, which means that the sum of the mass densities of the two components is regarded as a constant.

3.1. Statics

We here assume that a single rigid spherical particle is fixed in the mixture at the equilibrium to introduce the ψ -dependent part of the free-energy functional. It is given by

$$F[\psi] = \int_{V^e} d\mathbf{x} \left[f(\psi) + \frac{1}{2}M(\psi)|\nabla\psi|^2 \right] + \int_{\partial V} dS f_s(\psi) , \quad (3.1)$$

where ψ depends on the spatial position \mathbf{x} . The first term on the right-hand side above is the volume integral over the mixture region V^e , while the second term is the surface integral over the particle surface ∂V . The definitions of $f(\psi)$ and $M(\psi)$ are given below. The surface energy density, denoted by $f_s(\psi)$, is assumed to be linear with respect to ψ ; we suppose that the preferential adsorption is caused by such a short-range interaction as the hydrogen bond. The surface field is defined as $h = -f'_s(\psi)$; the prime hereafter indicates the derivative with respect to the variable. In the Gaussian model, $f(\psi)$ is a

quadratic function and M is a constant. In the present study, as mentioned in Sect. 1, we employ the renormalized local functional theory (Okamoto & Onuki 2012), where f is given by

$$f(\psi) \equiv k_{\text{B}}T_c \left(\frac{1}{2}C_1\xi_0^{-2}\omega^{\gamma-1}\tau\psi^2 + \frac{1}{12}C_1C_2\xi_0^{-2}\omega^{\gamma-2\beta}\psi^4 \right). \quad (3.2)$$

This is obtained after coarse-graining up to the local correlation length, for which we write ξ . Hereafter, $\alpha, \beta, \gamma, \nu$, and η are the critical exponents for binary mixtures near the demixing critical point (or in the three-dimensional Ising model), C_1 is a positive nonuniversal constant, and C_2 is given by

$$C_2 = 3u^*C_1\xi_0. \quad (3.3)$$

Here, ξ_0 denotes a nonuniversal microscopic length, and u^* denotes the scaled coupling constant at the Wilson-Fisher fixed point. We have $u^* = 2\pi^2/9$ in the three dimensions at the 1-loop order. The "distance" from the criticality is represented by a dimensionless quantity ω , which is defined to give

$$\xi = \xi_0\omega^{-\nu}. \quad (3.4)$$

A self-consistent condition gives

$$\omega = \tau + C_2\omega^{1-2\beta}\psi^2, \quad (3.5)$$

which leads to $\xi_\infty = \xi_0\tau^{-\nu}$ because the composition is critical far from the particle. The coefficient of the square gradient term in (3.1) equals

$$M = k_{\text{B}}T_c C_1\omega^{-\eta\nu}. \quad (3.6)$$

Thus, M is a positive function of ψ at a given temperature.

The order-parameter fluctuation is significant only on the length scales smaller than ξ . On larger length-scales, the probability distribution of the order-parameter profile should have a sharp peak around its maximum, and thus the most probable profile is regarded as observed without fluctuation (Okamoto & Onuki 2012; Yabunaka *et al.* 2013; Yabunaka & Onuki 2017). Hence, in the renormalized local functional theory, we can obtain this profile by minimizing (3.1), which is regarded as the grand-potential functional with the chemical potential μ , conjugate to ψ , being put equal to zero; μ vanishes because of the critical composition ($\psi = 0$) far from the particle. We thus find the equilibrium profile to satisfy

$$0 = f'(\psi) - \frac{1}{2}M'(\psi)|\nabla\psi|^2 - M(\psi)\Delta\psi \quad \text{in } V^e, \quad (3.7)$$

whose left-hand side implies $\mu = 0$, and

$$0 = h + M\mathbf{n} \cdot \nabla\psi \quad \text{at } \partial V, \quad (3.8)$$

where \mathbf{n} is the unit normal vector on the surface towards outside the particle. The equilibrium profile can deviate from zero near the particle surface because of the preferential adsorption.

We here assume that the preferential adsorption is represented by only the surface field and neglect higher-order terms with respect to ψ , such as the second-order term involving the surface enhancement (Bray & Moore 1977; Diehl 1986, 1997; Cardy 1996), to study how the adsorption influences the drag coefficient, as in the previous studies of the renormalized local functional theory or the deviation of the drag coefficient (Okamoto & Onuki 2012; Yabunaka *et al.* 2013; Yabunaka & Onuki 2017; Yabunaka *et al.* 2015; Okamoto *et al.* 2013; Furukawa *et al.* 2013; Fujitani 2018).

3.2. Dynamics

In the equilibrium, like an inhomogeneous magnetic field for a magnetic system, μ can be assumed to depend on \mathbf{x} . Under inhomogeneous chemical potential, assuming no bulk phase separation, still we can obtain the coarse-grained equilibrium profile by minimizing the grand-potential functional. Conversely, for a given coarse-grained profile $\psi(\mathbf{x})$, (3.1) gives the free-energy functional, and $\mu(\mathbf{x})$ is given by its functional derivative with respect to $\psi(\mathbf{x})$.

In the dynamics with the local equilibrium, the chemical potential μ is thus still given by the left-hand side of (3.7), *i.e.*,

$$\mu(\mathbf{x}, t) = f'(\psi) - \frac{1}{2}M'(\psi)|\nabla\psi|^2 - M(\psi)\Delta\psi \quad \text{for } \mathbf{x} \in V^e, \quad (3.9)$$

and (3.8) holds as it is. The latter is mentioned at (62c) of (Diehl & Janssen 1992) and in Appendix A of (Okamoto *et al.* 2013). Hereafter, $\psi(\mathbf{x}, t)$ represents the coarse-grained profile of the order parameter.

Considering the change in the free-energy functional due to the quasi-static deformation of the mixture, we can obtain the reversible part of the stress tensor (Onuki 2002), as is done in the model H. Writing $\mathbf{\Pi}$ for its negative, we have

$$\mathbf{\Pi} = \left(-f + \mu\psi - \frac{M}{2}|\nabla\psi|^2 \right) \mathbf{1} + M\nabla\psi\nabla\psi. \quad (3.10)$$

Without the composition gradient, the above gives a better-known expression of the osmotic pressure exerted on a semipermeable membrane $\psi f' - f$, which is mentioned in (de Gennes 1979) for example. The velocity field in the mixture \mathbf{v} still satisfies the first entry of (2.1). Because of

$$\nabla \cdot \mathbf{\Pi} = \psi \nabla \mu, \quad (3.11)$$

we can regard \mathbf{v} as satisfying

$$0 = -\nabla p - \psi \nabla \mu + \eta_o \Delta \mathbf{v}, \quad (3.12)$$

instead of the second entry of (2.1). The inertia term vanishes for the same reason as mentioned in Sect. 2; the pressure p still plays a role of keeping the incompressibility. The viscosity η_o is assumed to be homogeneous, considering the weak dependence of its singular part on ξ (Ohta 1975; Ohta & Kawasaki 1976). This point is discussed in Sect. 6. The diffusive flux between the two components is proportional to the gradient of μ , and the mass conservation of each component leads to

$$\frac{\partial}{\partial t} \psi(\mathbf{x}, t) = -\mathbf{v} \cdot \nabla \psi + \nabla \cdot [L(\psi) \nabla \mu]. \quad (3.13)$$

The first and second terms on the right-hand side above represent the mass transport due to the convection and the one due to the diffusion, respectively. The Onsager coefficient $L(> 0)$, depending on ξ , is regarded as a function of ψ at a given temperature, and is further discussed in Sect. 4.2. Equations (3.12) and (3.13), together with the first entry of (2.1), describe the hydrodynamics of the mixture on length scales larger than ξ (Yabunaka *et al.* 2015; Fujitani 2017).

As in Sect. 2, we assume that the particle undergoes translational motion with a constant velocity $\varepsilon U \mathbf{e}_z$ in a quiescent fluid, and proceed with calculations without making the physical meaning of ε explicit. A possible meaning is discussed in Sect. 6. The boundary conditions for \mathbf{v} are the same as described in Sect. 2. The diffusion flux cannot

pass across the particle surface, which leads to

$$L\partial_r\mu = 0 \text{ for } r = a \quad \text{and} \quad \mu \rightarrow 0 \text{ as } r \rightarrow \infty . \quad (3.14)$$

The first entry of (3.14) comes because the diffusive flux is defined on the frame co-moving with the particle. The surface boundary condition for ψ is given by (3.8); ψ approaches zero far from the particle. This and the second entry of (3.14) come because of the critical composition far from the particle. Viewed from the co-moving frame, the fields are stationary, and thus (3.13) leads to

$$[\mathbf{v} - \varepsilon U \mathbf{e}_z] \cdot \nabla \psi = \nabla \cdot [L(\psi) \nabla \mu] . \quad (3.15)$$

3.3. Set up for calculations

In the reference state at $\varepsilon = 0$, the particle center is fixed at the origin and the ambient mixture is quiescent, as in (Fujitani 2018). In this state, ψ can be calculated from (3.7) and (3.8) with ∂V being located at $r = a$; we write $\psi^{(0)}(r)$ for this solution, considering the rotational symmetry of the reference state. Over the mixture in this state, μ vanishes and p equals a constant, for which we write $p^{(0)}$. In addition to (2.3), we define $\psi^{(1)}$ and $\mu^{(1)}$ so that

$$\psi(\mathbf{x}) = \psi^{(0)}(r) + \varepsilon \psi^{(1)}(\mathbf{x}) \quad \text{and} \quad \mu(\mathbf{x}) = \varepsilon \mu^{(1)}(\mathbf{x}) \quad (3.16)$$

hold up to the order of ε . The fields with the superscript ⁽¹⁾ all vanish far from the particle. The time variable t is not explicitly written here for the same reason as mentioned in Sect. 2. Because of the symmetry of the particle motion, we have (2.4), (2.5), and

$$\mu^{(1)}(\mathbf{x}) = Q_{10}(r) Y_{10}(\theta) , \quad (3.17)$$

whereby Q_{10} is defined. In addition to (2.8), we introduce dimensionless functions

$$\mathcal{Q}(\rho) = \frac{Q_{10}(r) \sqrt{L(0)}}{U \sqrt{\eta_0}} \sqrt{\frac{3}{20\pi}} , \quad (3.18)$$

and

$$\Psi(\rho) = -\frac{r^2}{3\sqrt{5\eta_0}L(0)} \frac{d\psi^{(0)}(r)}{dr} , \quad (3.19)$$

where $L(0)$ is $L(\psi)$ for $\psi = 0$. We rewrite the r and θ components of (3.12) at the order of ε by using (2.3)–(2.5), (3.16) and (3.17). Using the same procedure that leads to (2.7), we here instead obtain

$$(\rho\partial_\rho + 1)(\rho\partial_\rho - 2)(\rho\partial_\rho + 3)\rho\partial_\rho\mathcal{R}(\rho) = -30\Psi(\rho)\mathcal{Q}(\rho) . \quad (3.20)$$

Equation (3.15) yields

$$(\rho\partial_\rho - 1)(\rho\partial_\rho + 2)\mathcal{Q}(\rho) = -3\Psi(\rho)[A(\rho)(\mathcal{R}(\rho) - 1) - B(\rho)\partial_\rho\mathcal{Q}(\rho)] , \quad (3.21)$$

where A and B are defined as

$$A(\rho) = \frac{L(0)}{L(\psi^{(0)}(a\rho))} \quad \text{and} \quad B(\rho) = \frac{L'(\psi^{(0)}(a\rho))}{aL(\psi^{(0)}(a\rho))} \sqrt{5\eta_0 L(0)} . \quad (3.22)$$

We have (2.10), while (3.14) gives

$$\partial_\rho\mathcal{Q} = 0 \text{ for } \rho = 1 \quad \text{and} \quad \mathcal{Q} \rightarrow 0 \text{ as } \rho \rightarrow \infty . \quad (3.23)$$

Regarding (3.20) as an equation for \mathcal{R} , we use (2.10) to have

$$\mathcal{R}(\rho) = 1 + \alpha_0(\rho) + \int_1^\infty d\sigma \Gamma_R(\rho, \sigma) \Psi(\sigma) \mathcal{Q}(\sigma) , \quad (3.24)$$

where the kernel Γ_R is given in Appendix and α_0 is defined by (2.11). Without the preferential adsorption, Ψ and \mathcal{Q} vanishes, and \mathcal{R} becomes $1 + \alpha_0$, as described in Sect. 2. Regarding (3.21) as an equation for \mathcal{Q} , we use (3.23) to have

$$\mathcal{Q}(\rho) = \int_1^\infty d\sigma \Gamma_Q(\rho, \sigma) \Psi(\sigma) [A(\sigma)(\mathcal{R}(\sigma) - 1) - B(\sigma)\partial_\sigma \mathcal{Q}(\sigma)] , \quad (3.25)$$

where the kernel Γ_Q is shown in Appendix.

Instead of the integral of (2.12) over the particle surface, the z component of the drag force is given by (Fujitani 2014, 2016)

$$\int_{\partial V} dS \mathbf{e}_z \cdot \left(-\mathbf{\Pi} \cdot \mathbf{e}_r + \nabla_{\parallel} f_s - \frac{2f_s}{a} \mathbf{e}_r - p\mathbf{1} \cdot \mathbf{e}_r + 2\eta_0 \mathbf{E} \cdot \mathbf{e}_r \right) , \quad (3.26)$$

where ∇_{\parallel} denotes the projection of ∇ on the tangent plane and $1/a$ is the mean curvature of the particle surface. The two terms involving f_s in (3.26) are canceled with each other after the integration, and thus need not be considered here, as mentioned in Appendix A of (Fujitani 2014). Writing $\varepsilon \mathbf{\Pi}^{(1)}$ for $\mathbf{\Pi}$ at the order of ε , we need to calculate the left-hand side of (3.27) below in calculating the contribution from the first term in the parentheses of (3.26) to γ_d . Because of (3.10), $\mathbf{\Pi}^{(1)}$ contains $\psi^{(1)}$, which satisfies (3.8) and (3.9). It is natural that the distortion of the order-parameter profile from the equilibrium one should contribute to $\Delta\gamma_d$. Thus, it appears that, even after we have solved $\mathcal{R}(\rho)$ and $\mathcal{Q}(\rho)$ for a given $\Psi(\rho)$ to find $\mathbf{v}^{(1)}$ and $\mu^{(1)}$, we still have to obtain $\psi^{(1)}$ from (3.8) and (3.9) in advance to calculate γ_d . However, this calculation can be evaded. We have

$$\begin{aligned} \int_{\partial V} dS \mathbf{e}_z \cdot \left(-\mathbf{\Pi}^{(1)} \cdot \mathbf{e}_r \right) &= \int_{V^e} d\mathbf{x} \psi^{(0)} \partial_z \mu^{(1)} \\ &= - \int_{\partial V} dS \left[\mu^{(1)} \psi^{(0)} \right] \cos \theta - \int_{V^e} d\mathbf{x} \mu^{(1)} \psi^{(0)'} \cos \theta , \end{aligned} \quad (3.27)$$

where the two equalities are derived with the aid of (3.11) and Gauss' divergence theorem. The formula given by (3.27) is helpful because its right-hand side does not contain $\psi^{(1)}$ and we need not obtain $\psi^{(1)}$ from (3.8) and (3.9). The formula is essentially the same as used at (37) of (Fujitani 2018), where the author calculated the quantity corresponding with $\psi^{(1)}$ by solving a linear differential equation to derive the formula in the Gaussian model. This derivation cannot be applied in the present formulation because an analytical expression of $\psi^{(1)}$ cannot be derived from (3.9), which is highly nonlinear with respect to ψ . Equation (3.27) gives an alternative and much simpler derivation, which is valid in cases more general than the previous derivation, including the present formulation.

The rest terms in the integrand of (3.26) involve p and \mathbf{E} . The latter is rewritten in terms of \mathcal{R} through the definition of \mathbf{E} . The former at the order of ε is related to \mathcal{R} with the aid of the θ component of (3.12), and contains the term coming from $-\psi \nabla \mu$, which is canceled by the first term on the right-hand side of (3.27) in calculating (3.26) at the order of ε . Thus we can use (3.24) and (3.26) to obtain

$$\gamma_d = 6\pi\eta_0 a \left(1 + \frac{10}{3} \int_1^\infty d\rho \alpha_0(\rho) \mathcal{Q}(\rho) \Psi(\rho) \right) \quad (3.28)$$

with the aid of (A 2). The second term in the parentheses above gives $\Delta\gamma_d$ divided by $6\pi\eta_0 a$ of the Stokes law. The quotient is below referred to as the normalized deviation, denoted by $\Delta\hat{\gamma}_d$. Instead of using (A 2), we can use the Lorentz reciprocal theorem (Lorentz 1896) to derive (3.28), as shown in Appendix B of (Fujitani 2018).

4. Elements of the calculation procedure

Our task is to calculate the drag coefficient by means of (3.28). For this, we should calculate \mathcal{Q} by determining the dependence of L on ψ and by obtaining $\psi^{(0)}$. How to carry out these steps are mentioned in the following subsections. To obtain \mathcal{Q} , we should solve the simultaneous equations with respect to \mathcal{R} and \mathcal{Q} , (3.24) and (3.25). Simultaneous equations of the same type are derived in the Gaussian model in (Fujitani 2018), where the derivative of the difference in the mass densities in the reference state, corresponding with $\psi^{(0)'} in the present study, is proportional to the surface field and a series expansion with respect to a dimensionless surface field is naturally introduced. In contrast, in the present formulation, $\Psi \propto \psi^{(0)' in (3.24) and (3.25) is not proportional to h . Thus, in Sect. 4.1, we introduce an artificial parameter to derive a series expansion of the solution.$$

4.1. Calculation for \mathcal{Q}

We modify (3.24) and (3.25) by replacing Ψ with $\kappa\Psi$, where κ is the artificial parameter. The solutions of these modified equations become dependent on κ , and are denoted by $\tilde{\mathcal{R}}(\rho, \kappa)$ and $\tilde{\mathcal{Q}}(\rho, \kappa)$. The original solutions, $\mathcal{R}(\rho)$ and $\mathcal{Q}(\rho)$, are respectively equal to $\tilde{\mathcal{R}}(\rho, 1)$ and $\tilde{\mathcal{Q}}(\rho, 1)$. Substituting the modified equation from (3.24), *i.e.*,

$$\tilde{\mathcal{R}}(\rho, \kappa) = 1 + \alpha_0(\rho) + \kappa \int_1^\infty d\sigma \Gamma_R(\rho, \sigma) \Psi(\sigma) \tilde{\mathcal{Q}}(\sigma, \kappa) , \quad (4.1)$$

into the modified equation from (3.25), *i.e.*,

$$\tilde{\mathcal{Q}}(\rho, \kappa) = \kappa \int_1^\infty d\sigma \Gamma_Q(\rho, \sigma) \Psi(\sigma) \left[A(\sigma) \left(\tilde{\mathcal{R}}(\sigma, \kappa) - 1 \right) - B(\sigma) \partial_\sigma \tilde{\mathcal{Q}}(\sigma, \kappa) \right] , \quad (4.2)$$

gives an integral equation with respect to $\tilde{\mathcal{Q}}$.

Writing $\tilde{q}_1, \tilde{q}_2, \dots$ for the expansion coefficients, we assume

$$\tilde{\mathcal{Q}}(\rho, \kappa) = \sum_{n=1}^{\infty} \tilde{q}_n(\rho) \kappa^n , \quad (4.3)$$

which is substituted into the integral equation with respect to $\tilde{\mathcal{Q}}$ to yield the recurrence relations for the expansion coefficients. The difference in the braces of (4.2) equals $A(\sigma)\alpha_0(\rho)$ at the order of κ^0 , and we obtain

$$\tilde{q}_1(\rho) = \int_1^\infty d\sigma \Gamma_Q(\rho, \sigma) \Psi(\sigma) A(\sigma) \alpha_0(\sigma) . \quad (4.4)$$

Similarly, we pick up the terms at the order of κ^n ($n = 2, 3, \dots$) from the integral equation to obtain

$$\tilde{q}_2(\rho) = - \int_1^\infty d\sigma \Gamma_Q(\rho, \sigma) \Psi(\sigma) B(\sigma) \frac{\partial}{\partial \sigma} \tilde{q}_1(\sigma) , \quad (4.5)$$

and

$$\tilde{q}_n(\rho) = \int_1^\infty d\sigma \left[\Gamma(\rho, \sigma) \Psi(\sigma) q_{n-2}(\sigma) - \Gamma_Q(\rho, \sigma) \Psi(\sigma) B(\sigma) \frac{\partial}{\partial \sigma} q_{n-1}(\sigma) \right] \quad (4.6)$$

for $n = 3, 4, \dots$, where the kernel Γ is defined as

$$\Gamma(\rho, \sigma) = \int_1^\infty d\tau \Gamma_Q(\rho, \tau) \Psi(\tau) A(\tau) \Gamma_R(\tau, \sigma) . \quad (4.7)$$

Substituting (4.3) with $\kappa = 1$ into (3.28) gives

$$\Delta\hat{\gamma}_d = \sum_{n=1}^{\infty} \chi_n, \quad (4.8)$$

where χ_n is defined as

$$\chi_n = \frac{10}{3} \int_1^{\infty} d\rho \alpha_0(\rho) \tilde{q}_n(\rho) \Psi(\rho). \quad (4.9)$$

4.2. Dependence of L on the order parameter

In this paragraph, we consider the near-critical fluctuation about the equilibrium in the absence of a particle; ξ is homogeneous. Here, the thermal average of the composition in the mixture is uniform but not necessarily equal to the critical one; $\varphi(\mathbf{x}, t)$ represents the fluctuating composition and $\delta\varphi(\mathbf{x}, t)$ is defined as $\varphi(\mathbf{x}, t) - \bar{\varphi}$, where $\bar{\varphi}$ denotes the thermal average of φ . We write $C_{\mathbf{k}}(t)$ for the spacial Fourier transform of the correlation function, *i.e.*, the thermal average of $\delta\varphi(\mathbf{x}, t)\delta\varphi(\mathbf{0}, 0)$, with \mathbf{k} denoting the wave-number vector. In the mode-coupling theory (Kawasaki 1970; Swinney & Henry 1973; Onuki 2002), the convection at smaller length scales is regarded as a part of the diffusion at larger length scales, which leads to

$$\frac{\partial}{\partial t} C_{\mathbf{k}}(t) = -\frac{k_B T_c}{6\pi\eta_0\xi} |\mathbf{k}|^2 C_{\mathbf{k}}(t) \quad (4.10)$$

for small wave-number $|\mathbf{k}| \lesssim \xi^{-1}$. Here, the regular part is assumed to be much smaller than the singular part. The fraction in (4.10) gives the diffusion coefficient in a coarse-grained picture, where the convection does not contribute to the mass transport. The time derivative of $\delta\varphi$ on large length-scales should be also given by the second term on the right-hand side of (3.13) with $L(\psi)$ being regarded as $L(\bar{\varphi})$. Then, we can approximate μ of (3.9) to be $f'(\psi)$ for long wave-length fluctuations, and rewrite the second term as $Lf''(\psi)\Delta\delta\varphi(\mathbf{x}, t)$. Multiplying this term with $\delta\varphi(\mathbf{0}, 0)$ and taking the thermal average of the product, we should find that the Fourier transform of the average equals the right-hand side of (4.10). For this to hold, Lf'' should be approximately equal to the fraction in (4.10) for $|\mathbf{k}|\xi \ll 1$.

Let us turn back to our calculation of the drag coefficient. We assume that the equality mentioned at the end of the preceding paragraph locally holds when the particle moves in the mixture. Thus, in calculating γ_d , we use

$$L(\psi) = \frac{k_B T}{6\pi\eta_0\xi f''(\psi)}, \quad (4.11)$$

where f'' is the inverse susceptibility. The approximation introduced here presupposes small spatial variation of ψ . At least, the variation of $L(\psi)$ over ξ is required to be small as compared with its typical value at every locus. From (3.2) and (3.5), we derive

$$f'(\psi) = k_B T_c C_2 \psi \omega^\gamma \frac{2 - \alpha + 4(1 - \alpha)\tau\omega^{-1} + 5\alpha\tau^2\omega^{-2}}{18u^* [2\beta + (1 - 2\beta)\tau\omega^{-1}] \xi_0^3}. \quad (4.12)$$

Similarly, we can calculate $f''(\psi)$, although its lengthy expression is not shown here. This expression tells

$$f''(\psi) \rightarrow k_B T_c C_1 \tau^\gamma \xi_0^{-2} \quad \text{as } \psi \rightarrow 0, \quad (4.13)$$

which leads to

$$L(0) = \frac{\xi_0}{6\pi\eta_0 C_1 \tau^{\gamma-\nu}}. \quad (4.14)$$

The scaling relation for the critical exponents gives $\gamma \approx 2\nu$ because of $\eta \approx 0.036 \ll 2$ for three-dimensional binary fluid (Pelissetto & Vicari 2002), and thus $L(0)$ is approximately proportional to ξ_∞ . In more general, considering that f'' gives the inverse of the susceptibility involving the critical exponent γ , the scaling relation and (4.11) approximately lead to $L \propto \xi$. This linearity is expected in view of the mode-coupling theory, although the power is found to be slightly smaller than unity in the dynamic renormalization group calculation (Siggia *et al.* 1976).

4.3. Dimensionless parameters and the equilibrium profile

We numerically calculate the equilibrium profile, $\psi^{(0)}(r)$, by solving (3.7) and (3.8) in combination with (3.5), as was done in (Okamoto & Onuki 2013). Equation (3.4) then gives ξ . Some dimensionless parameters are introduced below to facilitate numerical calculations. A characteristic reduced temperature τ_a is defined so that ξ becomes a for $\psi = 0$ at $\tau = \tau_a$. A characteristic order parameter ψ_a is defined so that ξ becomes a for $\psi = \psi_a$ at $\tau = 0$. Equation (3.5) gives

$$\tau_a = (\xi_0/a)^{1/\nu} \quad \text{and} \quad \psi_a = \tau_a^\beta / \sqrt{C_2}. \quad (4.15)$$

The reduced temperature and order parameter are respectively scaled as $\hat{\tau} \equiv \tau/\tau_a$ and $\hat{\psi}(\rho) \equiv \psi(a\rho)/\psi_a$. Introducing a dimensionless surface field, defined as

$$\hat{h} = \frac{ha\sqrt{C_2}}{k_B T_c C_1 \tau_a^\beta}, \quad (4.16)$$

we can rewrite (3.8) as

$$\partial_\rho \hat{\psi}^{(0)}(\rho) = -\hat{h}\omega^{\nu\eta} \quad \text{at } \rho = 1, \quad (4.17)$$

where $\hat{\psi}^{(0)}(\rho)$ is defined as $\psi^{(0)}(a\rho)/\psi_a$. Noting (3.19) and (4.14), we find

$$\Psi(\rho) = -\frac{\rho^2}{\sqrt{5\pi\hat{\tau}^{\nu-\gamma}}} \frac{d\hat{\psi}^{(0)}(\rho)}{d\rho}. \quad (4.18)$$

We use $\nu = 0.627$; see (Pelissetto & Vicari 2002) for the values of the critical exponents. Unless otherwise stated, we hereafter put $\eta = 0$ for simplicity, considering its small positive value mentioned above. This allows us to take M as a constant $k_B T_c C_1$ because of (3.6). Equations (3.7) and (4.12) give

$$\begin{aligned} & (\partial_\rho^2 + 2\rho^{-1}\partial_\rho) \hat{\psi}^{(0)}(\rho) \\ &= \frac{[2 - \alpha + 4(1 - \alpha)\hat{\tau}\hat{\omega}^{-1} + 5\alpha\hat{\tau}^2\hat{\omega}^{-2}] \hat{\omega}^\gamma}{6[2\beta + (1 - 2\beta)\hat{\tau}\hat{\omega}^{-1}]} \hat{\psi}^{(0)}(\rho) \quad \text{for } \rho > 1, \end{aligned} \quad (4.19)$$

where $\hat{\omega}$ is defined as ω/τ_a and satisfies $\hat{\omega} = \hat{\tau} + \hat{\omega}^{1-2\beta}\hat{\psi}^2$ because of (3.5). We numerically solve (4.17) with η being put equal to zero and (4.19) by using Mathematica (Wolfram) to obtain $\hat{\psi}^{(0)}$, and then $\Psi(\rho)$ with the aid of (4.18). When η vanishes, (4.17) does not involve ω , and thus we can proceed with the calculation only by fixing the values of \hat{h} and $\xi_\infty/a = \hat{\tau}^{-\nu}$. Otherwise, the value of τ_a should be fixed in addition. The scaling relations for the critical exponents for $\eta = 0$ are

$$\alpha = 2 - 3\nu, \quad \beta = \nu/2, \quad \text{and} \quad \gamma = 2\nu. \quad (4.20)$$

Figure 1 shows how the equilibrium order-parameter profile and the local correlation length depend on $\rho = r/a$. Far from the particle, the former approaches zero, which represents the critical composition, and the latter approaches the prescribed value of

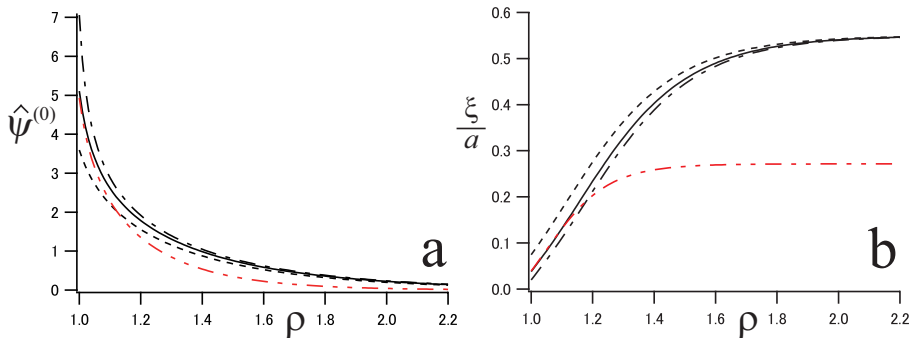


FIGURE 1. The normalized order parameter (a) and correlation length (b) are plotted against the dimensionless radial distance $\rho \equiv r/a$. Dash, solid, and dot-dash curve represent the results for $\xi_{\infty}/a = 0.55$, and respectively for $\hat{h} = 24, 60$, and 150 . Two-dot chain (red) curve represents the result for $\xi_{\infty}/a = 0.27$ and $\hat{h} = 60$.

ξ_{∞}/a . Near the particle surface, the preferred component is more concentrated and the correlation length becomes smaller as \hat{h} increases. The stronger adsorption makes the mixture near the surface more off-critical. At a distance of ξ_{∞} from the particle surface, $\psi^{(0)}$ is approximately reduced to ψ_a . The local correlation length ξ should be smaller than the local length scale that the flow changes, denoted here by l , for the validity of the hydrodynamics formulated from the coarse-grained free-energy density. In the flow at a distance r from the center of a particle moving translationally, l would be equal or larger than r . In Fig. 1(b), ξ is significantly small as compared with r . Thus, the hydrodynamics in the present formulation is available in calculating the drag coefficient for the parameter values examined.

It is known that the Gaussian free-energy density can describe the static properties only when the mixture is not so much close to the critical point. The proportionality of $\xi \propto \tau^{-\nu}$ with $\nu \approx 0.627$ is observed in the bulk of a binary fluid mixture with the critical composition when it is sufficiently close to the critical point. The Gaussian free-energy density, giving $\xi \propto \tau^{-0.5}$ instead, appears to be valid when ξ is smaller than approximately 15 nm in the bulk of the mixture of 2, 6-lutidine and water (Jungk *et al.* 1987). When the particle motion is studied in the Gaussian model (Okamoto *et al.* 2013; Fujitani 2018), the correlation length is assumed to be homogeneous and much smaller than the minimum of l , *i.e.*, approximately a , for the validity of the hydrodynamics based on the free-energy density. Thus, the Gaussian model is valid for small ξ_{∞} (< 15 nm in the example above) and $\xi_{\infty}/a \ll 1$. The present formulation is not tied to these constraints.

In Fig. 2(a), ξ at the surface (denoted by ξ_1) is approximately equal to ξ_{∞} for small ξ_{∞}/a , and reaches a plateau after a slight peak as ξ_{∞}/a increases. The plateau of ξ_1 indicates that $\hat{\psi}^{(0)}$ at the surface becomes independent of ξ_{∞}/a . The discrepancy between ξ_1 and ξ_{∞} implies the inhomogeneity in ξ , and cannot be described by the Gaussian model. As \hat{h} increases in Fig. 2(a), the inhomogeneity appears at smaller ξ_{∞}/a and the plateau value is smaller, which is expected because the preferential adsorption causes the inhomogeneity. At the critical point ($\xi_{\infty} = \infty$), the equilibrium profile around a spherical particle is calculated in (Yabunaka & Onuki 2017), where ξ_1/a is found to be given by $6^{-1/3}\hat{h}^{-2/3}$ for $\hat{h} \gg 1$. This theoretical result respectively gives $\xi_1/a = 6.6, 3.6$, and 1.9×10^{-2} for $\hat{h} = 24, 60$, and 150 . The values of ξ_1/a on the extreme right in Fig. 2(a) are 7.4, 3.8, and 2.0×10^{-2} for these values of \hat{h} , respectively. The latter two agree well

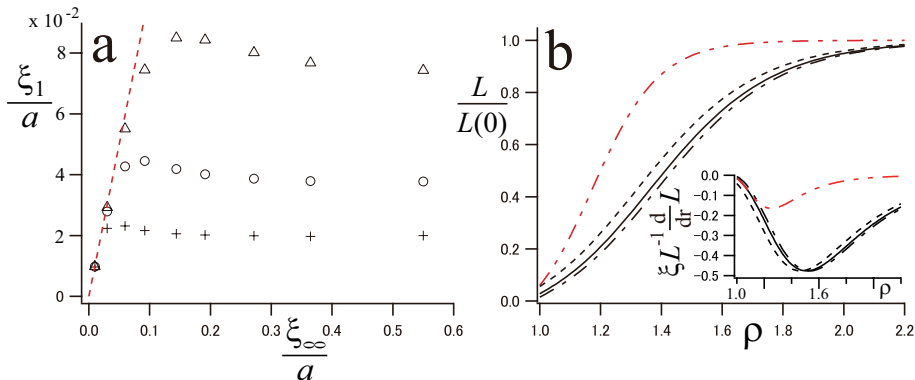


FIGURE 2. (a) The normalized correlation length at the particle surface ξ_1/a is plotted against ξ_∞/a for $\hat{h} = 24$ (\triangle), 60 (\circ), and 150 ($+$). Dash line (red) represents $\xi_1 = \xi_\infty$. (b) The ratio $L(\psi^{(0)}(\rho a))/L(0)$ is plotted against ρ . The normalized change of $L(\psi^{(0)}(r))$ over ξ , represented by $\xi L^{-1} dL/(dr)$, is plotted against $\rho \equiv r/a$ in the inset. The parameter values for each curve are the same as used in Fig. 1.

with the corresponding theoretical results, showing the strong adsorption ($\tau \ll \omega$ at the surface). Depending on the values of a and \hat{h} , it is possible that the inhomogeneity occurs to invalidate the Gaussian model even when the Gaussian free-energy density gives good approximation to static properties in the bulk. Judging from Fig. 2(a), when a equals 100 nm, the inhomogeneity begins to occur at the value of ξ_∞ smaller than 10 nm for the strong adsorption. At this small value of ξ_∞ , the Gaussian free-energy density can describe the correlation length in the bulk of the mixture of 2, 6-lutidine and water, which is mentioned in the preceding paragraph and is also discussed in Sect. 6.

The Onsager coefficient $L(\psi^{(0)})$ increases as $\psi^{(0)}$ approaches zero, which is shown in Fig. 2(b). At a distance of ξ_∞ from the particle surface, $L(\psi^{(0)}(r))$ increases to become approximately 70 % of its value far from the particle, $L(0)$. Judging from Figs. 1(a) and 2(b), as is known, ξ_∞ gives a typical thickness of the adsorption layer. The inset of Fig. 2(b) shows $\xi L^{-1} dL/(dr)$, whose absolute value represents how large the variation of $L(\psi)$ over ξ , mentioned below (4.11), is as compared with the local value of $L(\psi)$. The absolute value is sufficiently small for $\hat{h} = 60$ over the region of ρ examined, while it is still smaller than unity but becomes rather large around $\rho = 1.5$ for $\hat{h} = 150$.

5. Results

We truncate (4.8) appropriately to calculate $\Delta\hat{\gamma}_d$. The change of the partial sum occurring when the number of the terms (N) increases by one becomes smaller than 1% of the partial sum for $N \geq 109$ in Fig. 3. In this example, we can regard the partial sum of $N = 109$ as the infinite sum. As \hat{h} or ξ_∞/a increases, we need larger N to evaluate the infinite sum with the same accuracy, although data not shown. The numerical results shown later are obtained using N smaller than approximately 100. Some improvements to reduce the numerical cost are desirable when N is required to be significantly larger than 100.

It is shown in Fig. 4 how $\Delta\hat{\gamma}_d$ changes as the critical temperature is approached. The deviation increases with \hat{h} and ξ_∞/a , as is expected because it is caused by the adsorption. In this figure, for small ξ_∞/a , $\Delta\hat{\gamma}_d$ appears to be approximately proportional to the fourth power of ξ_∞/a . As ξ_∞/a increases in Fig. 4(a), the slope shown by each of the symbols,

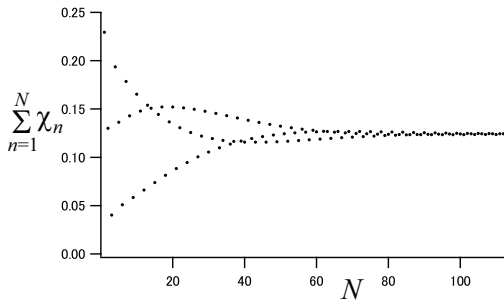


FIGURE 3. Plot of $\chi_1 + \chi_2 + \dots + \chi_N$ against N for $\hat{h} = 150$ and $\xi_\infty/a = 0.36$.

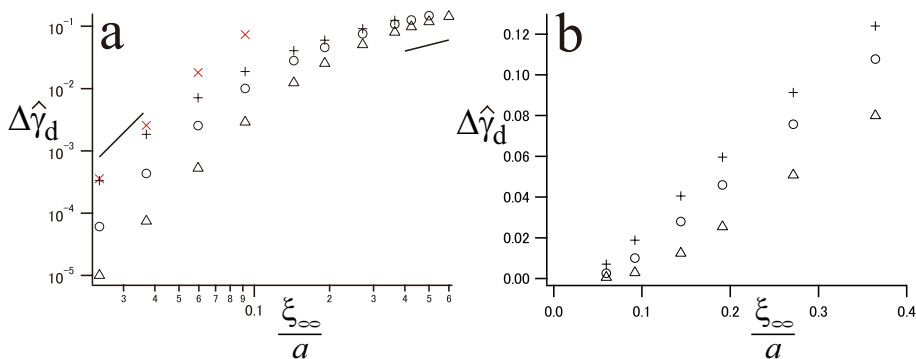


FIGURE 4. (a) Logarithmic and (b) linear plots of the normalized deviation of the drag coefficient $\Delta \hat{\gamma}_d$ against ξ_∞/a for $\hat{h} = 24(\Delta)$, $60(\circ)$, and $150(+)$. Each of the results is obtained using a partial sum of (4.8). Lines in (a) represent the slopes of one and four. The symbol \times (red) in (a) represents the results in the Gaussian model for $\hat{h} = 150$.

$+$, \circ , and Δ , becomes more gradual and the dependence appears to shift to the linear dependence; the shift occurs at larger ξ_∞/a as \hat{h} decreases. For large ξ_∞/a in Fig. 4(b), $\Delta \hat{\gamma}_d$ appears to be a linear function of ξ_∞/a , whose slope is calculated from the two data points on the right end to give 0.31, 0.34, and 0.35 for $\hat{h} = 24, 60, 150$, respectively. This suggests that the slope should become insensitive to \hat{h} as ξ_∞/a increases. The approximate fourth-power dependence for smaller ξ_∞/a , shown in Fig. 4(a), is mentioned at the end of the penultimate paragraph of Sect. 4 of (Fujitani 2018), where the Gaussian model is studied and the parameter $\Lambda(\approx \hat{h}/\sqrt{5\pi})$ is used. For reference in Fig. 4(a), using the calculation procedure in (Fujitani 2018), we plot the normalized deviation in the Gaussian model, corresponding with $\Delta \hat{\gamma}_d$, for $\hat{h} = 150$; the results (\times) deviate upward from the results of the present study ($+$) as ξ_∞/a increases.

By assuming L to be homogeneous, instead of using (4.11), we calculate $\Delta \hat{\gamma}_d$ to obtain the symbols of \times in Fig. 5(a). This drastic change in modeling L does not influence $\Delta \hat{\gamma}_d$ for smaller values of ξ_∞/a , and reduces $\Delta \hat{\gamma}_d$ slightly as ξ_∞/a increases. It is unchanged that the dependence of $\Delta \hat{\gamma}_d$ on ξ_∞/a becomes more gradual than in the Gaussian model. We thus expect that the appearance of the gradual dependence should be robust against the details of the dependence of L on ψ , although the results in the inset of Fig. 2(b) suggest that (4.11) is not completely reliable especially for $\hat{h} = 150$.

As mentioned in Sect. 1, some researchers regard the deviation of γ_d as caused by effective enlargement of the particle radius due to the adsorption layer. However, for the parameter values examined in Fig. 5(b), the change of v_θ/U at $\theta = \pi/2$ due to the

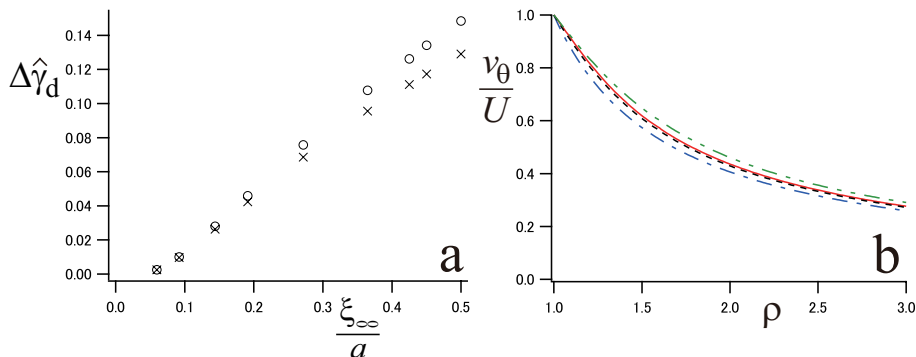


FIGURE 5. (a) The normalized deviation $\Delta\hat{\gamma}_d$ is obtained for $\hat{h} = 60$ by assuming (4.11) (○) and by assuming L to be homogeneous (×). Some of the results shown by ○ are shared with Fig. 4. (b) The tangential component of the velocity field v_θ divided by U is plotted against ρ on the equatorial plane $\theta = \pi/2$. Dot-dash curve (blue) represents the results in the absence of the preferential adsorption ($h = 0$). Dash, solid, and two-dot chain curves (black, red, and green, respectively) represent the results for $(\hat{h}, \xi_\infty/a) = (60, 0.19)$, $(150, 0.19)$, and $(60, 0.36)$, respectively.

preferential adsorption is smaller than approximately 20 % of v_θ/U in its absence; the velocity field is not so much changed by the preferential adsorption and the mixture fluid in the adsorption layer cannot be regarded as a part of the rigid particle. The velocity gradient at the surface becomes more gradual as ξ_∞/a increases, which suggests reduction in the viscous stress exerted on the particle. The velocity field is influenced by \mathbf{II} because of (3.11) and (3.12). How \mathbf{II} changes with ξ_∞/a influences on how $\Delta\hat{\gamma}_d$ changes with ξ_∞/a not only directly through the first term in the parentheses of (3.26) but also through the last two terms by changing the flow field.

The dependence of $\Delta\hat{\gamma}_d$ on ξ_∞/a becomes close to the linear one in Fig. 4(a) in the range of $(\hat{h}, \xi_\infty/a)$ showing the inhomogeneity of ξ in Fig. 2(a). This is reasonable because of the close relationship between $\psi^{(0)}$ and $\Delta\gamma_d$ shown by (3.28). In Fig. 2(a), the inhomogeneity occurs approximately when ξ_1/a exceeds ξ_∞/a . Thus, when large \hat{h} causes the strong adsorption, the dependence in Fig. 4(a) becomes close to the linear one if we have

$$\frac{\xi_\infty}{a} > 6^{-1/3} \hat{h}^{-2/3}. \quad (5.1)$$

6. Discussion

The Gaussian free-energy density was used in the previous studies on the drag coefficient (Okamoto *et al.* 2013; Fujitani 2018). There, ξ_∞ should be sufficiently small so that the free-energy density can describe the static properties in the bulk and so that the correlation length can be regarded as homogeneous. The latter condition can require smaller ξ_∞ than the former unless the adsorption is weak. Thus, the Gaussian model is not always available in calculating γ_d even if the static properties in the mixture bulk can be described by the Gaussian free-energy density, as mentioned in Sect. 4.3. The free-energy density in (3.1) is completely free from these conditions because it can describe the static properties in the bulk even at the critical point and the inhomogeneity of ξ . This inhomogeneity is correlated with the appearance of the approximate linearity between $\Delta\hat{\gamma}_d$ and ξ_∞/a , which should occur for large ξ_∞/a satisfying (5.1).

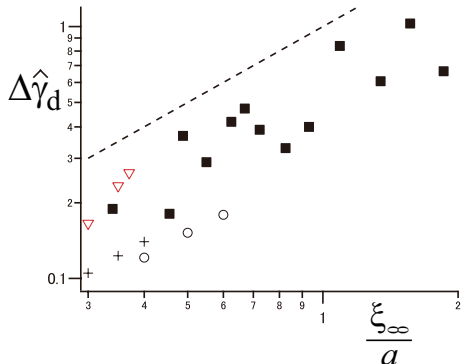


FIGURE 6. Solid squares represent part of the data in the top of Fig. 2 of (Omari *et al.* 2009). Circles and crosses represent our results calculated with $\eta = 0.036$ for $\hat{h} = 60$ and 150, respectively. The calculated values are slightly larger for large ξ_∞/a than the ones obtained with $\eta = 0$. For $(\hat{h}, \xi_\infty/a) = (60, 0.4)$ and $(60, 0.5)$, we have $\Delta\hat{\gamma}_d = 0.119$ (0.121) and 0.148 (0.152) by using $\eta = 0$ (0.036), respectively. The triangles (red) represent the results for $\hat{h} = 24$ in the Gaussian model. Dash line represents $\Delta\hat{\gamma}_d = \xi_\infty/a$.

Omari *et al.* (Omari *et al.* 2009) measured the self-diffusion of silica particles in a near-critical mixture of 2,6-lutidine and water, for which T_c is approximately 307 K (Gülari *et al.* 1972; Jungk *et al.* 1987). The former is preferentially adsorbed by the particle, and the self-diffusion coefficient is suppressed as T_c is approached. The data on the top of Fig. 2 of (Omari *et al.* 2009), except the data point on the extreme left, are replotted in Fig. 6; $a = 25$ nm and $\xi_0 = 0.25$ nm used in this reference lead to $\tau_a = 6.5 \times 10^{-4}$. We thus have $\xi_\infty/a = 0.76$ for $\tau = 10^{-3}$; the replotted data range from $\tau = 3.6 \times 10^{-3}$ to 2.3×10^{-4} . Equations (4.15) and (4.16) give $\hat{h} = h\sqrt{3u^*a^3}/(k_B T_c \sqrt{C_1})$ for $\eta = 0$. The value of h may be usually smaller than 10^{-5} m³/s², considering the following three points; (1) a typical energy of the hydrogen bond is 10^{-20} J per a molecule, (2) the area of the particle surface interacting with one molecule of the mixture would be larger than approximately 1 nm², and (3) $|\psi|$ is at most 10^3 kg/m³. Using a typical value of M for alkanes, 10^{-16} m⁷/(kg · s²) (Carey *et al.* 1980; Cornelisse *et al.* 1996), we find that \hat{h} is smaller than approximately 160. We use a partial sum of (4.8) with $\eta = 0.036$ to calculate $\Delta\hat{\gamma}_d$, and plot the results for small values of ξ_∞/a in Fig. 6. We did not calculate $\Delta\hat{\gamma}_d$ at values of ξ_∞/a larger than shown in the figure for each of $\hat{h} = 60$ and 150 because of heavy numerical costs. The calculation results for $h = 60$ and 150 appear to have almost the same slopes with the slope suggested by the experimental data. However, judging from Fig. 6, the calculation would yield smaller $\Delta\hat{\gamma}_d$ than the experimental data, even if performed for the same values of ξ_∞/a that gives the experimental data. The underestimation may be attributed to our assumption of homogeneous viscosity.

The singular part of the viscosity is proportional to $\xi^{1/19}$ up to the 1-loop order (Ohta 1975; Ohta & Kawasaki 1976; Siggia *et al.* 1976). Thus, its nonuniversal regular part, which can depend on the local composition, is not negligible unless the mixture is very close to the critical point. We can estimate $\psi_a \approx 15$ kg/m³ for the parameter values mentioned above, using (3.3), (3.6) and (4.15). Considering that mass density of 2, 6-lutidine (0.93 g/cm³) is almost the same as that of water, the change of 5% in the weight percent of 2, 6-lutidine in the mixture approximately amounts to that of 7 in $\hat{\psi}^{(0)}$. In Fig. 1(a), the values of $\hat{\psi}^{(0)}$ at the surface are approximately 5 and 7 for $\hat{h} = 60$ and 150 for $\xi_\infty/a = 0.55$, respectively. The data of the viscosity for various values of the

weight percent are shown at $\tau \approx 10^{-2}$ and 10^{-4} in (Stein *et al.* 1972). From them, in the experimental system yielding the data replotted in Fig. 6, the viscosity near the surface is guessed to be raised by approximately 30 % around $\tau = 10^{-3}$. It is thus possible that the underestimation suggested in Fig. 6 can be explained by this slight increase of the viscosity in the adsorption layer. The viscosity may be regarded as homogeneous over the mixture around $\tau = 10^{-4}$ due to the overlap of the regular and singular parts, according to the data in (Stein *et al.* 1972). These data also suggest that, when τ is smaller than 10^{-4} , or ξ_∞ is larger than approximately 80 nm, the singular part should become more explicit to cause inhomogeneous viscosity.

The results in the Gaussian model for $\hat{h} = 150$ in Fig. 4(a) are obtained using a series expansion with respect to the dimensionless parameter proportional to h , which is mentioned in the preface of Sect. 4; the series is given by the first entry of (47) in (Fujitani 2018). For $\hat{h} = 24, 60$ and 150 , respectively, when ξ_∞/a is larger than approximately 0.4, 0.18 and 0.1, the drag coefficient cannot be calculated in the Gaussian model because the expansion series is numerically divergent. Results in the Gaussian model for $\hat{h} = 24$ are plotted with triangles in Fig. 6. For $\hat{h} = 60$ and $\xi_\infty/a = 0.14$, the normalized deviation in the Gaussian model is 8.3×10^{-2} , and is larger than the corresponding result shown by the circle in Fig. 4(a). Thus, as far as examined, the dependence of the normalized deviation of the drag coefficient on ξ_∞/a in the Gaussian model does not become close to the linear one, in contrast to our results calculated with the renormalized local functional theory. It is to be noted that, judging from Fig. 2(a), the Gaussian model loses validity for $\hat{h} = 24, 60$, and 150 in the range of ξ_∞/a of Fig. 6. It is thus only for reference that the results in the Gaussian model are plotted in this figure. If the particle were enlarged by the thickness of the adsorption layer, we would have $\Delta\hat{\gamma}_d = \xi_\infty/a$, which is also plotted for reference in Fig. 6. This naive idea clearly oversimplifies the dynamics of the mixture; it is suggested by Fig. 5(b) that the mixture generally flows in the adsorption layer. That the dash line lies above the experimental data in Fig. 6 may imply that the naive idea could be justified approximately if the preferred component were extremely viscous.

The particle radius in the experiment is rather small. For $a = 25$ nm, our coarse-grained picture should become less reliable very near the surface because ξ_1 reaches a microscopic length scale in Fig. 1(b). Our theory can be safely applied to the particle radius larger than approximately 100 nm. Lee (Lee 1976) measured the self-diffusion coefficient of such large particles in a ternary mixture near the plait point, and found out the linear dependence of $\Delta\hat{\gamma}_d$ on ξ_∞/a when τ is approximately smaller than 3×10^{-2} (*i.e.*, $\xi_\infty \gtrsim 5$ nm). For this mixture, the renormalized local functional theory is available if τ is replaced by a variable proportional to $\tau^{1/(1-\alpha)}$ (Fisher 1968; Folk & Moser 1995), although the definition of the surface field and (3.13) should be modified for ternary mixtures.

In Fig. 1(b), ξ is much smaller than a near the particle, and increases to approach ξ_∞ mainly in the region of $r - a < \xi_\infty$. Thus, for the parameter values examined, ξ nowhere exceeds the length scale that the flow changes (l), which would be equal or larger than r . In particular when the adsorption strong, the local correlation length near the particle is much smaller than the particle radius. Thus, when we consider a large particle ($a \gtrsim 100$ nm) with the strong adsorption in a near-critical mixture whose ξ_∞ is not so large as to cause explicit singular part of the viscosity ($\xi_\infty < 80$ nm in the mixture mentioned above), l is sufficiently large as compared with ξ everywhere. Then, we can use the present hydrodynamic formulation based on the coarse-grained free-energy density in calculating the drag coefficient, without considering the critical fluctuations significant on length scales smaller than ξ .

We use ε as a convenient parameter to calculate the drag coefficient up to the linear order with respect to the particle speed. The parameter is taken as representing the Reynolds number in deriving the conventional Stokes law, which holds for the low Reynolds number, as mentioned in Sect. 2. Thus, we can discuss the validity range of the linear regime by making the physical meaning of ε explicit. In the presence of the preferential adsorption in the near criticality, the low Reynolds number should remain required for the linearity, but it would not be sufficient because nonlinearity is suggested to be made relevant by significant distortion of the adsorption layer due to the particle motion (Furukawa *et al.* 2013). The distortion would be reduced by the mutual diffusion of the two fluid components, while augmented by the convection. The time scale that the former occurs over the adsorption layer can be estimated to be $(a + \xi_\infty)^2/D$, where D is the diffusion coefficient given by the fraction in (4.10), while the one for the latter to be $a + \xi_\infty$ divided by the particle speed U_o . Thus, ε in our problem would be taken as representing not only the Reynolds number but also the Péclet number, $(a + \xi_\infty)U_o/D$, which increases with ξ_∞ . It is to be noted that we calculate the drag force by taking into account the distortion of the adsorption layer, as mentioned above (3.27). However, elucidating the validity range should require calculating beyond the linear regime and checking the linearity for various values of the parameters including ξ_∞ . To examine whether the Brownian motion can be described by a linear Langevin equation, we may need to study the drag force beyond the linear regime in the framework of the fluctuating hydrodynamics, considering that a Brownian particle does not always move translationally in a quiescent fluid. It is thus well expected that the self-diffusion coefficient of a Brownian particle should not always follow Einstein's relation, *i.e.*, should not be always given by $k_B T/\gamma_d$, even when the Reynolds number is sufficiently small. The relation can break down when ξ_∞/a is sufficiently large. We believe that our results of the drag coefficient should also give a firm basis to some future works, experimental or theoretical, on the validity range of ξ_∞/a for Einstein's relation in the presence of the preferential adsorption in the near-criticality.

Acknowledgements

S. Y. was supported by Grant-in-Aid for Young Scientists (B) (15K17737 and 18K13516).

Appendix A. Some details

The kernel appearing in (3.24) is given by

$$\Gamma_R(\rho, \sigma) = \begin{cases} \frac{(3-5\sigma^2)}{2\sigma^3\rho^3} + 5\frac{(3\sigma^2-1)}{2\sigma^3\rho} + \sigma^2\rho^{-3} - 5\rho^{-1} & \rho \geq \sigma \\ \frac{(3-5\sigma^2)}{2\sigma^3\rho^3} + 5\frac{(3\sigma^2-1)}{2\sigma^3\rho} + \rho^2\sigma^{-3} - 5\sigma^{-1} & \sigma \geq \rho. \end{cases} \quad (\text{A1})$$

We find

$$\left(\frac{1}{2}\partial_\rho^3 + 2\partial_\rho^2\right)\Gamma_R(\rho, \sigma) = 15[\alpha_0(\sigma) + 1], \quad (\text{A2})$$

at $\rho = 1$. The operator in the parentheses above appears in (2.13). The kernel appearing in (3.25) is given by

$$\Gamma_Q(\rho, \sigma) = \begin{cases} (\rho\sigma)^{-2}/2 + \rho\sigma^{-2} & \rho \leq \sigma \\ (\rho\sigma)^{-2}/2 + \sigma\rho^{-2} & \sigma \leq \rho. \end{cases} \quad (\text{A3})$$

These kernels are originally obtained in (Okamoto *et al.* 2013).

We can calculate the equilibrium profile numerically by using (3.7) and (3.8), as they are, after the non-dimensionalization mentioned in Sect. 4.3. Alternatively, we can utilize (A5) of (Fujitani 2016), whose $s(\psi(\rho))$ is defined by $\omega(\psi(\rho))/\tau - 1$ becomes proportional to $e^{-2\rho a/\xi_\infty}/\rho^2$ far from the particle. The differential equation with respect to the ratio of the former to the latter, that is $s(\psi(\rho))e^{2\rho a/\xi_\infty}\rho^2$, can be derived from (3.7), and is solved numerically under the boundary conditions imposed sufficiently far from the particle. At $\rho = 10$, we required the derivative of s with respect to ρ to vanish, and fixed the value of s so that \hat{h} becomes a prescribed value with the aid of (3.8).

REFERENCES

- BAL'TSEVICH, YA. A., MARTYNETS, V. G. & MATIZEN, E. V. 1967 Brownian motion at the critical point of two-phase liquid-liquid equilibrium. *Sov. Phys. JETP* **24**, 654.
- BARBOT, A. & ARAKI, T. 2017 Colloidal suspensions in one-phase mixed solvents under shear flow. *Softmatter* **13**, 5911.
- BEDAUX, D. & MAZUR, P. 1974 Brownian motion and fluctuating hydrodynamics. *Physica A* **76** 247.
- BERTSEVA, E., GREBENKOV, D., SCHMIDHAUSER, P., GRIBKOVA, S., JENEY, S. & FORRÓ, L. 2012 Optical trapping microrheology in cultured human cells. *Eur. Phys. J. E* **35**, 63.
- BEYSENS, D. 2019 Brownian motion in strongly fluctuating liquid. *Thermodynamics of Interfaces and Fluid Mechanics* **3**, 1–8.
- BEYSENS, D. & ESTÈVE, D. 1985 Adsorption phenomena at the surface of silica spheres in a binary liquid mixture. *Phys. Rev. Lett.* **54**, 2123.
- BEYSENS, D. & LEIBLER, S. 1982 Observation of an anomalous adsorption in a critical binary mixture. *J. Physique Lett.* **43**, 133–136.
- BIAN, X, KIM, C. & KARNIADAKIS, G. E. 2016 111 years of brownian motion. *Soft Matter* **12**, 6331–6346.
- BINDER, M. N. 1983 *Phase Transitions and Critical Phenomena VIIIIV*, chap. Critical behavior at surfaces. Academic, London.
- BONN, D, OTWINOWSKI, J, SACANNA, S, GUO, H, WEGDAM, G & SCHALL, P. 2009 Direct observation of colloidal aggregation by critical casimir forces. *Phys. Rev. Lett.* **103**, 156101.
- BRAU, R. R., FERRER, J. M., LEE, H., CASTRO, C. E., TAM, B. K., TARSA, P. B., MATSUDAIRA, P., BOYCE, M. C., KAMM, R. D. & LANG, M. J. 2007 Passive and active microrheology with optical tweezers. *J. Opt. A: Pure Appl. Opt.* **9**, S103.
- BRAY, A. J. & MOORE, M. A. 1977 Critical behaviour of semi-infinite systems. *J. Phys. A: Math. Gen.* **10**, 1927.
- CAHN, J. W. 1977 Critical point wetting. *J. Chem. Phys.* **66**, 3667.
- CAMLEY, B. A. & BROWN, F. L. H. 2014 Fluctuating hydrodynamics of multicomponent membranes with embedded proteins. *J. Chem. Phys.* **141**, 075103.
- CARDY, J. 1996 *Scaling and Renormalization in Statistical Physics*, chap. 7. Cambridge Univ Press, Cambridge.
- CAREY, B. S., SCRIVEN, L. E. & DAVIS, H. T. 1980 Semiempirical theory of surface tension of binary systems. *AIChE J.* **26**, 705.
- CASE, K. M. 1971 Velocity fluctuations of a body in a fluid. *Phys. Fluids* **14**, 2091.
- CHESTER, W., BREACH, D. R. & PROUDMAN, I. 1976 On flow past a sphere at low Reynolds number. *J. Fluid Mech.* **37**, 751.
- CORNELISSE, P. M. W., PETERS, C. J. & DE SWAAN ARONS, J. 1996 Non-classical interfacial tension and fluid phase behaviour. *Fluid Phase Equilib.* **117**, 312.
- DIEHL, H. W. 1986 *Phase Transition and Critical Phenomena X*, chap. Field theoretical approach to critical behavior at surfaces. Academic, London.
- DIEHL, H. W. 1997 The theory of boundary critical phenomena. *Int. J. Mod. Phys. B* **11**, 3503.
- DIEHL, H. W. & JANSSEN, H. K. 1992 Boundary conditions for the field theory of dynamic critical behavior in semi-infinite systems with conserved order parameter. *Phys. Rev. A* **45**, 7145.

- DOMÍNGUEZ-GARCÍA, P., CARDINAUX, F., BERTSEVA, E., FORRÓ, L., SCHEFFOLD, F. & JENEY, S. 2014 Accounting for inertia effects to access the high-frequency microrheology of viscoelastic fluids. *Phys. Rev. E* **90**, 060301.
- EINSTEIN, A. 1905 On the motion of small particles suspended in liquids at rest required by the molecular-kinetic theory of heat. *Ann. Phys. (Leipzig)* **322**, 549.
- FISHER, M. E. 1968 Renormalization of critical exponents by hidden variables. *Phys. Rev.* **176**, 257.
- FISHER, M. E. & AU-YANG, H. 1980 Critical wall perturbations and a local free energy functional. *Physica A* **101**, 255.
- FOLK, R. & MOSER, G. 1995 Critical dynamics near plait points in mixtures. *J. Low Temp. Phys.* **99**, 11.
- FRANOSCH, T., GRIMM, M., BELUSHKIN, M., MOR, F. M., FOFFI, G., FORRÓ, L., & JENEY, S. 2011 Resonances arising from hydrodynamic memory in brownian motion. *Nature* **478**, 85.
- FUJITANI, Y. 2007 Connection of fields across the interface in the fluid particle dynamics method for colloidal dispersions. *J. Phys. Soc. Jpn.* **76**, 064401.
- FUJITANI, Y. 2014 Effective viscosity of a near-critical binary fluid mixture with colloidal particles dispersed dilutely under weak shear. *J. Phys. Soc. Jpn.* **83**, 084401.
- FUJITANI, Y. 2016 Fluctuation amplitude of a trapped rigid sphere immersed in a near-critical binary fluid mixture within the regime of the gaussian model. *J. Phys. Soc. Jpn.* **85**, 044401.
- FUJITANI, Y. 2017 Undulation amplitude of a fluid membrane in a near-critical binary fluid mixture calculated beyond the gaussian model supposing weak preferential attraction. *J. Phys. Soc. Jpn.* **86**, 044602.
- FUJITANI, Y. 2018 Osmotic effects on dynamics of a colloidal rigid sphere in a near-critical binary fluid mixture. *J. Phys. Soc. Jpn.* **87**, 084602.
- FURUKAWA, A., GAMBASSI, A., DIETRICH, S. & TANAKA, H. 2013 Nonequilibrium critical casimir effect in binary fluids. *Phys. Rev. Lett.* **11**, 055701.
- DE GENNES, P. G. 1979 *Scaling Concepts in Polymer Physics*, chap. Sect. III. 1. 3. Cornell Univ Press, Ithaca.
- GREBENKOV, D. S., VAHABI, M., BERTSEVA, E., FORRÓ, L. & JENEY, S. 2013 Hydrodynamic and subdiffusive motion of tracers in a viscoelastic medium. *Phys. Rev. E* **88**, 040701.
- GRIMM, M., FRANOSCH, T. & JENEY, S. 2012 High-resolution detection of brownian motion for quantitative optical tweezers experiments. *Phys. Rev. E* **86**, 021912.
- GÜLARI, E., COLLINGS, A. F., SCHMIDT, R. L. & PINGS, C. J. 1972 Light scattering and shear viscosity studies of the binary system 2, 6lutidinewater in the critical region. *J. Chem. Phys.* **56**, 6169.
- HOHENBERG, P. C. & HALPERIN, B. I. 1977 Theory of dynamic critical phenomena. *Rev. Mod. Phys.* **49**, 435.
- HOLYST, R. & PONIEWIERSKI, A. 1987 Wetting on a spherical surface. *Phys. Rev. B* **36**, 5628.
- HUANG, R., CHAVEZ, I., TAUTE, K. M., LUKIĆ, B., JENEY, S., RAIZEN, M. & FLORIN, E.-L. 2011 Direct observation of the full transition from ballistic to diffusive brownian motion in a liquid. *Nat. Phys.* **7**, 576.
- HUTTER, K. & Y. WANG 2016 *Fluid and Thermodynamics : Volume 2: Advanced Fluid Mechanics and Thermodynamic Fundamentals*, Chap. 11. Springer, Berlin.
- ITAMI, M. & S. SASA 2015 Derivation of Stokes' law from Kirkwood's formula and the Green-Kubo formula via large deviation theory. *J. Stat. Phys.* **161** 532
- JUNGK, M., BELKOURA, L. & WOERMANN, D. 1987 Study of a binary critical mixture of 2,6dimethyl pyridine/water: Measurements of static and dynamic light scattering and specific heat near the lower critical point. *Ber. Bunsenges. Phys. Chem.* **91**, 507.
- KAWASAKI, K. 1970 Kinetic equations and time correlation functions of critical fluctuations. *Ann. Phys. (N.Y.)* **61**, 1.
- KIMURA, Y. 2009 Microrheology of soft matter. *J. Phys. Soc. Jpn.* **78**, 041005.
- KUBO, R., TODA, M. & HASHITSUME, N. 1991 *Statistical Physics*, chap. 1.6. Springer, Berlin.
- LAMB, H. 1932 *Hydrodynamics*, Sect. 335. Dover, New York.
- LEE, S. P. 1976 Evidence for the "correlated layer" effect on the effective viscosity from brownian motion in a ternary liquid mixture. *Phys. Rev. Lett.* **36**, 1319.

- LORENTZ, H. A. 1896 A general theorem concerning the motion of a viscous fluid and a few consequences derived from it. *Versl. Kon. Akad. Wetensch. Amsterdam* **5**, 168.
- LUKIĆ, B., JENEY, S., TISCHER, C., KULIK, A. J., FORRÓ, L. & FLORIN, E.-L. 2005 Direct observation of nondiffusive motion of a brownian particle. *Phys. Rev. Lett.* **95**, 160601.
- LYONS, K. B., MOCKLER, R. C. & O'SULLIVAN, W. J. 1973 Light-scattering investigation of brownian motion in a critical mixture. *Phys. Rev. Lett.* **30**, 42.
- LYONS, K. B., MOCKLER, R. C. & O'SULLIVAN, W. J. 1974 Brownian motion in a critical mixture: k -dependent diffusion. *Phys. Rev. A* **10**, 393.
- MARTYNETS, V. G. & MATIZEN, E. V. 1970 Brownian motion near the critical point of the two-phase liquid-liquid equilibrium. *Sov. Phys. JETP* **31**, 228.
- MAZUR, P. & VAN DER ZWAN, G. 1978 Brownian motion in a fluid close to its critical point. *Physica* **92A**, 483.
- OHTA, T. 1975 Selfconsistent calculation of dynamic critical exponents for classical liquid. *Prog. Theor. Phys.* **54**, 1566.
- OHTA, T. & KAWASAKI, K. 1976 Mode coupling theory of dynamic critical phenomena for classical liquids. I: Dynamic critical exponents. *Prog. Theor. Phys.* **55**, 1384.
- OKAMOTO, R., FUJITANI, Y. & KOMURA, S. 2013 Drag coefficient of a rigid spherical particle in a near-critical binary fluid mixture. *J. Phys. Soc. Jpn* **82**, 084003.
- OKAMOTO, R. & ONUKI, A. 2012 Casimir amplitudes and capillary condensation of near-critical fluids between parallel plates: Renormalized local functional theory. *The Journal of Chemical Physics* **136**, 114704.
- OKAMOTO, R. & ONUKI, A. 2013 Attractive interaction and bridging transition between neutral colloidal particles due to preferential adsorption in a near-critical binary mixture. *Phys. Rev. E* **88**, 022309.
- OMARI, R. A., GRABOWSKI, C. A. & MUKHOPADHYAY, A. 2009 Effect of surface curvature on critical adsorption. *Phys. Rev. Lett.* **103**, 225705.
- ONUKI, A. 2002 *Phase Transition Dynamics*. Cambridge University Press.
- PELISETTO, A. & VICARI, E. 2002 Critical phenomena and renormalization-group theory. *Phys. Rep.* **368**, 549.
- PESCE, G., LUCA, A. C. DE, RUSCIANO, G., NETTI, P. A., FUSCO, S. & SASSO, A. 2009 Microrheology of complex fluids using optical tweezers: a comparison with macrorheological measurements. *J. Opt. A: Pure Appl. Opt.* **11**, 034016.
- SIGGIA, E. D., HOHENBERG, P. C. & HALPERIN, B. I. 1976 Renormalization-group treatment of the critical dynamics of the binary-fluid and gas-liquid transitions. *Phys. Rev. B* **13**, 2110.
- STEIN, A., DAVIDSON, S. J., ALLEGRA, J. C. & ALLEN, G. F. 1972 Tracer diffusion and shear viscosity for the system 2,6lutidinewater near the lower critical point. *J. Chem. Phys.* **56**, 6164.
- STOKES, G. G. 1851 On the effect of the internal friction of fluids on the motion of pendulums. *Trans. Cambridge Philos. Soc.* **9** (9).
- SUTHERLAND, W. 1905 Lxxv. a dynamical theory of diffusion for non-electrolytes and the molecular mass of albumin. *Philos. Mag* **781**.
- SWINNEY, H. & HENRY, D. L. 1973 Dynamics of fluids near the critical point: Decay rate of order-parameter fluctuations. *Phys. Rev. A.* **8**, 2586.
- TANI, H. & FUJITANI, Y. 2018 Drag coefficient of a circular inclusion in a near-critical binary fluid membrane drag coefficient of a circular inclusion in a near-critical binary fluid membrane. *J. Phys. Soc. Jpn.* **87**, 104601.
- WIDOM, A. 1971 Velocity fluctuations of a hard-core brownian particle. *Phys. Rev. A* **3**, 1394.
- YABUNAKA, S., OKAMOTO, R. & ONUKI, A. 2013 Phase separation in a binary mixture confined between symmetric parallel plates: Capillary condensation transition near the bulk critical point. *Phys. Rev. E* **87**, 032405.
- YABUNAKA, S., OKAMOTO, R. & ONUKI, A. 2015 namics in bridging and aggregation of two colloidal particles in a near-critical binary mixture. *Soft Matter* **11**, 5738.
- YABUNAKA, S. & ONUKI, A. 2017 Critical adsorption profiles around a sphere and a cylinder in a fluid at criticality: Local functional theory. *Phys. Rev. E* **96**, 032127.
- VAN DER ZWAN, G. & MAZUR, P. 1979 Brownian motion in a fluid near its critical point ii: The fluctuation-dissipation theorem. *Physica A* **98**, 169.

- ZWANZIG, R. & BIXON, M. 1970 Hydrodynamic theory of the velocity correlation function. *Phys. Rev. A* **2**, 2005.
- ZWANZIG, R. & BIXON, M. 1975 Compressibility effects in the hydrodynamic theory of Brownian motion. *J. Fluid Mech.* **69**, 21.